Switching 2D magnetic states via pressure tuning of layer stacking

Tiancheng Song^{1,9}, Zaiyao Fei^{1,9}, Matthew Yankowitz^{1,9}, Zhong Lin¹, Qianni Jiang¹, Kyle Hwangbo¹, Qi Zhang^{1,9}, Bosong Sun¹, Takashi Taniguchi³, Kenji Watanabe^{1,9}, Michael A. McGuire⁴, David Graf⁵, Ting Cao^{6,7}, Jiun-Haw Chu¹, David H. Cobden^{1,9}, Cory R. Dean², Di Xiao⁸ and Xiaodong Xu^{1,7,*}

The physical properties of two-dimensional van der Waals crystals can be sensitive to interlayer coupling. For twodimensional magnets¹⁻³, theory suggests that interlayer exchange coupling is strongly dependent on layer separation while the stacking arrangement can even change the sign of the interlayer magnetic exchange, thus drastically modifying the ground state⁴⁻¹⁰. Here, we demonstrate pressure tuning of magnetic order in the two-dimensional magnet Crl₃. We probe the magnetic states using tunnelling8,11-13 and scanning magnetic circular dichroism microscopy measurements². We find that interlayer magnetic coupling can be more than doubled by hydrostatic pressure. In bilayer Crl₃, pressure induces a transition from layered antiferromagnetic to ferromagnetic phase. In trilayer Crl₃, pressure can create coexisting domains of three phases, one ferromagnetic and two antiferromagnetic. The observed changes in magnetic order can be explained by changes in the stacking arrangement. Such coupling between stacking order and magnetism provides ample opportunities for designer magnetic phases and functionalities.

In a van der Waals (vdW) material, a relative shift of a fraction of a lattice constant between adjacent layers can cause a drastic change in certain physical properties. In particular, if the material is magnetic it can modify the interlayer exchange pathways leading to a change in the magnitude14 and sign of the interlayer exchange coupling⁴⁻⁸. For example, bulk two-dimensional (2D) magnet CrI₃ has monoclinic stacking at room temperature and undergoes a transition to rhombohedral stacking at 220 K (ref. 15). This stacking has been reported to display ferromagnetic interlayer coupling below the critical temperature of 61 K (Fig. 1a)¹⁵. On the other hand, thin exfoliated CrI₃ has been found to act as a layered antiferromagnetic insulator in which adjacent ferromagnetic monolayers are antiferromagnetically coupled. Second harmonic generation measurements have revealed a C_{2h} symmetry in bilayer CrI₃ (ref. ¹⁶),(consistent with recent theoretical proposals that antiferromagnetic coupling is associated with monoclinic layer stacking⁴⁻⁸ (Fig. 1b). Recently, puncturing of a thin flake of CrI₃ by a diamond probe tip at low temperature was found to switch the magnetic state from antiferromagnetic to ferromagnetic¹⁷, suggesting that mechanical force can change layer stacking. These findings highlight the opportunity provided by vdW magnets for realization of new magnetic configurations by controlling the layer stacking arrangement.

Hydrostatic pressure can be used for continuous control of interlayer coupling via interlayer spacing in vdW crystals. This has recently been shown to modify the bands in graphene/hexagonal boron nitride (hBN) moiré superlattices¹⁸ and transition metal dichalcogenides^{19,20}, as well as correlated electronic phases in twisted bilayer graphene²¹. Pressure has also been applied to a number of bulk vdW magnets, successfully altering the critical temperature^{22–25}. Here, by applying pressure to bi- and trilayer CrI₃, we demonstrate marked tuning of the critical field for spin-flip transition by control of interlayer spacing, as well as switching of interlayer magnetic order via pressure-induced structural transition.

Figure 1c shows a schematic of the experimental set-up. A magnetic tunnel junction (MTJ) device is composed of a bi- or trilayer CrI₃ sandwiched by top and bottom multilayer graphene contacts. The entire MTJ is encapsulated by hBN to prevent sample degradation. The device is then held in a piston cylinder cell for application of hydrostatic pressure up to 2.7 GPa. Magnetic states are probed in situ using tunnelling measurements. After removal from the cell, reflective magnetic circular dichroism (RMCD) microscopy is performed on the samples with a helium–neon laser. All measurements are performed at a temperature of 2 K in an out-of-plane magnetic field (see Methods for details).

We first present results from a bilayer CrI_3MTJ (device 1). Figure 1d shows the tunnelling current, I_0 , versus magnetic field, H, swept up and down, at a series of pressures. At zero pressure it shows the typical behaviour of a layered antiferromagnetic bilayer $^{8,11-13}$. Below 0.6 T, the two individual ferromagnetic layers in series form an antialigned spin filter that suppresses the tunnelling current to form a plateau. As the field is increased, a spin-flip transition occurs to a fully polarized state with a higher tunnelling current.

As the pressure is increased the critical field for spin-flip transition rises dramatically, to >1.3 T (Figs. 1d and 2a), more than double its zero-pressure value. Such an enhancement can be explained by reduced interlayer spacing, which increases the wavefunction overlap and thus the interlayer exchange strength^{4–8}. $I_{\rm t}$ also increases substantially with pressure owing to reduced interlayer spacing. In contrast, the critical temperature, $T_{\rm c}$, increases only slightly (Fig. 2a and Supplementary Fig. 1), consistent with it being determined mainly by intralayer exchange interactions that are relatively independent of interlayer spacing. Note that the steady background decrease in $I_{\rm t}$ with magnetic field is due to positive magnetoresistance in the multilayer graphene contacts²⁶. This background

¹Department of Physics, University of Washington, Seattle, WA, USA. ²Department of Physics, Columbia University, New York, NY, USA. ³National Institute for Materials Science, Tsukuba, Japan. ⁴Materials Science and Technology Division, Oak Ridge National Laboratory, Oak Ridge, TN, USA. ⁵National High Magnetic Field Laboratory, Tallahassee, FL, USA. ⁶Geballe Laboratory for Advanced Materials, Stanford University, Stanford, CA, USA. ⁷Department of Materials Science and Engineering, University of Washington, Seattle, WA, USA. ⁸Department of Physics, Carnegie Mellon University, Pittsburgh, PA, USA. ⁹These authors contributed equally: Tiancheng Song, Zaiyao Fei. *e-mail: xuxd@uw.edu

NATURE MATERIALS LETTERS

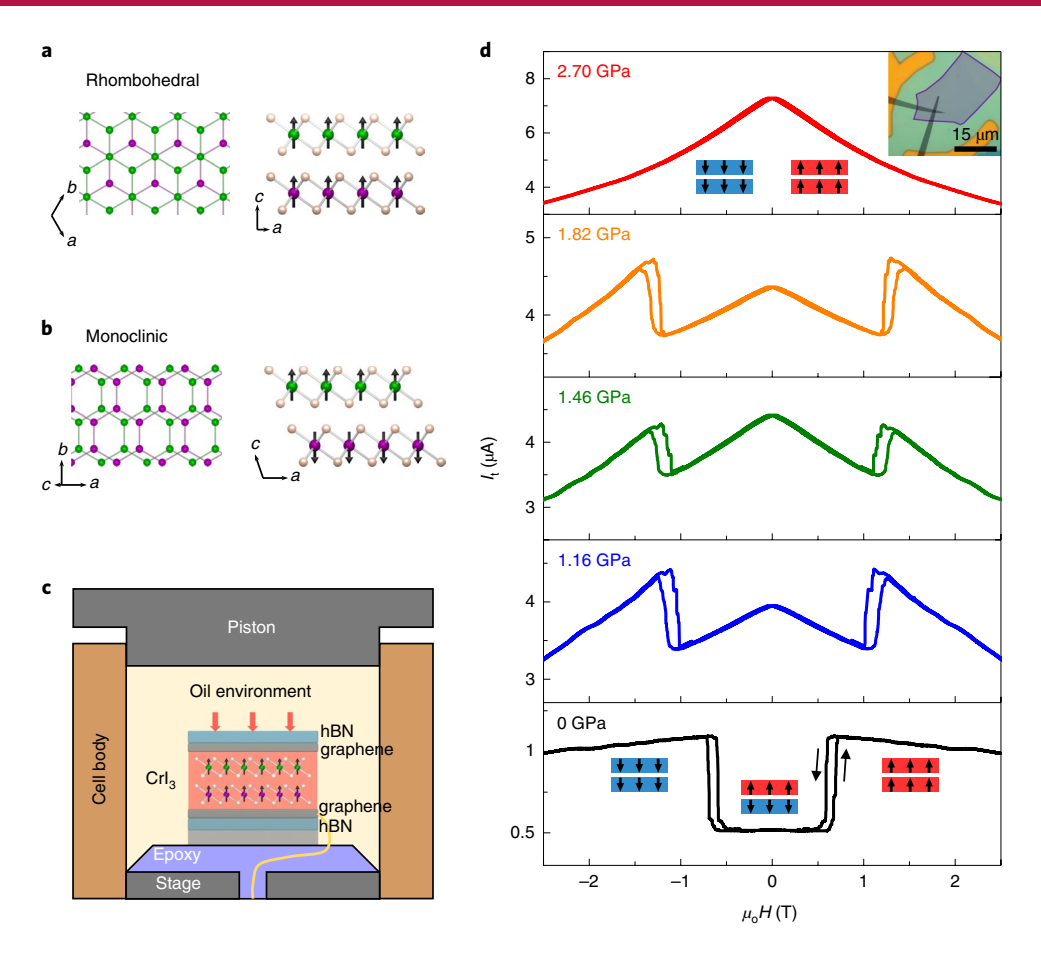


Fig. 1 | Stacking-order determined 2D magnetism and tunnelling measurements of bilayer Crl₃ under pressure. a, Schematic of rhombohedral stacking with top (left) and side view (right) indicating the ferromagnetic interlayer coupling. The green (purple) atoms represent the Cr atoms in the top (bottom) layer while the brown ones represent the I atoms. Here, *a*, *b* and *c* represent the axes of the crystal. **b**, Schematic for monoclinic stacking, indicating antiferromagnetic interlayer coupling. **c**, Schematic of high-pressure experimental set-up. A Crl₃ MTJ device is held in a piston pressure cell. The yellow line embedded in epoxy represents electrical leads. The force applied to the piston exerts a pressure on the device through oil (red arrows). **d**, Tunnelling current, *l*_v, versus magnetic field, *H*, at a series of pressures. Insets: magnetic states (only one of the two time-reversal AFM ground states is shown) and optical microscopy image of a bilayer MTJ (device 1) with junction area <1µm². Purple and grey shaded areas denote bilayer Crl₃ and graphene contacts, respectively; the yellow and green regions denote gold contacts and hBN flakes, respectively. Applied direct current bias, 50 mV.

magnetoresistance becomes more noticeable as the tunnelling magnetoresistance of CrI₃ is reduced—that is, at higher pressures.

Importantly, at the highest pressure of 2.7 GPa, the increase in I versus H due to spin-flip transition is absent, not due to the critical field moving out of the magnetic field sweeping range, and only the background multilayer graphene magnetoresistance remains. Figure 2b compares the temperature dependence of the zero-bias tunnelling conductance at $\mu_0 H = 0$ before application of pressure (black) with that at 2.7 GPa (red). Initially at zero pressure there is a kink near 44 K, consistent with T_c reported for the layered antiferromagnet bilayer². Below T_c , I_t decreases on cooling due to strengthening antiferromagnetic order. In contrast, at 2.7 GPa, I, increases on cooling, indicative of ferromagnetic order. In fact, this temperature dependence is similar to that of the fully spin-polarized state with $\mu_0 H = 1.5 \text{ T}$ applied at zero pressure (Supplementary Fig. 1a). These observations taken together imply that bilayer CrI₃ has switched from a layered antiferromagnetic state at low pressure to a ferromagnetic state at high pressure.

To further support this conclusion, we performed RMCD measurements after removal of the devices from the pressure cell. Device 1 was found to be broken, so RMCD was performed on a second bilayer device (device 2) which had been cycled to a comparable pressure (2.45 GPa) and temperature. Figure 2c shows

the ambient pressure RMCD signal at 2K, which exhibits a single pronounced hysteresis loop centred at $\mu_0 H = 0$, characteristic of ferromagnetism (see Supplementary Fig. 2 for the full dataset). This is distinct from the vanishing RMCD signal from a pristine CrI₃ bilayer (Fig. 2d)². Figure 2e shows the Raman spectra of a pristine bilayer (black trace) and of device 2 following pressure (red trace), taken at 80 K. Compared to the pristine samples, the peaks near 77 and 105 cm⁻¹ are blue- and red-shifted by about 0.8 and 0.6 cm⁻¹, respectively. This is consistent with Raman studies of CrI3 bulk crystals, in which these peaks shift in a similar manner by about 1 cm⁻¹ as a structural transition occurs from rhombohedral to monoclinic^{27,28}. Moreover, the peak near 105 cm⁻¹ corresponds to a twofold degenerate E_{o} mode for rhombohedral stacking. It splits into non-degenerate A_{α} and B_{α} modes for monoclinic stacking due to lower symmetry. This can be characterized by a fourfold polarization dependence of this peak in the pristine bilayer, which is absent in the bilayer after pressure (see Supplementary Fig. 3). Since these different stacking arrangements of CrI₃ have opposite signs of interlayer exchange, we infer that high pressure induces an irreversible structural transition in bilayer CrI₃.

Having demonstrated pressure control of magnetic order in bilayers, we now consider trilayer CrI₃. A pristine exfoliated trilayer has two layered antiferromagnetic ground states, which we now

LETTERS NATURE MATERIALS

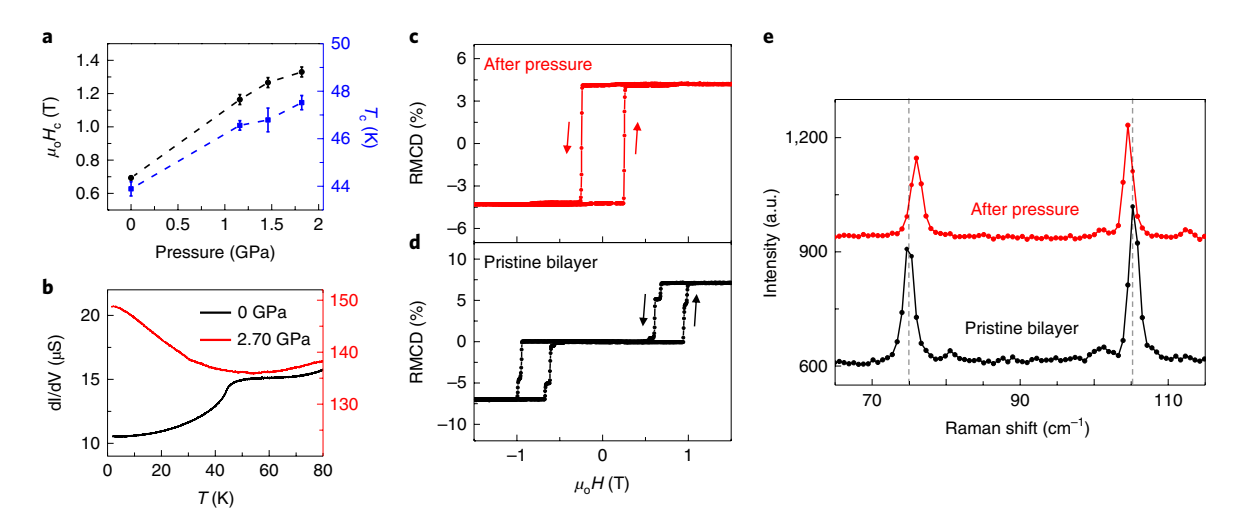


Fig. 2 | Effect of pressure on the magnetic properties of bilayer Crl₃. a, Extracted critical field for spin-flip transition (black circles) and critical temperature (blue squares) as a function of pressure. The error bar for the critical field is determined by the half-width of the spin-flip transition. For critical temperature, the error bar is determined by the temperature range over which dG/dT drops to 80% of peak value. **b**, Zero-bias tunnelling conductance versus temperature at zero pressure (black) and 2.7 GPa (red). **c,d**, RMCD signal from another bilayer (device 2) after removal from pressure cell where it was subjected to comparable pressure (2.45 GPa) and a thermal cycle to device1 (**c**), and from a pristine bilayer Crl₃ (**d**). **e**, Raman spectra of bilayer device 2 after pressure (red trace) and of a pristine bilayer (black trace) in the parallel polarization channel. a.u., arbitrary units. Data are vertically shifted for clarity.

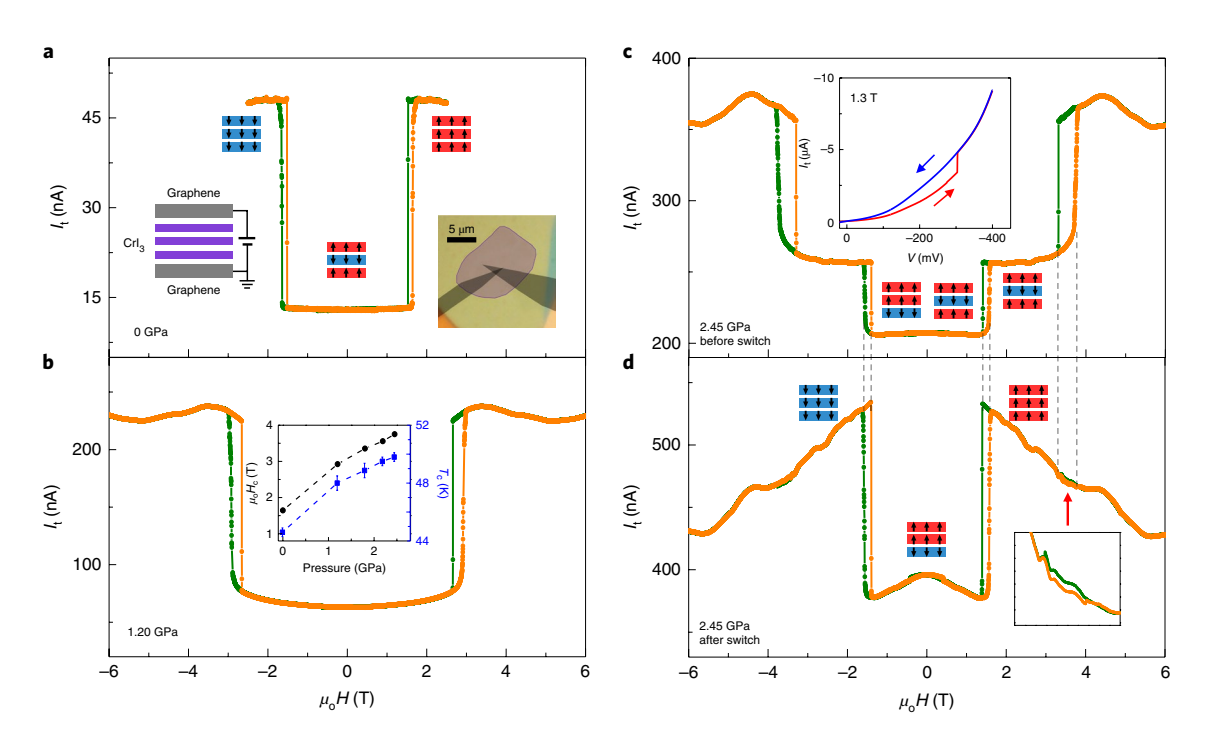


Fig. 3 | New pressure-induced magnetic states in trilayer Crl₃. a,b, Tunnelling current as a function of magnetic field at zero pressure (**a**) and 1.2 GPa (**b**). Applied bias, 70 mV. Insets in **a** are schematics indicating magnetic states—measurement geometry (bottom left) and an optical microscopy image of device 3 (bottom right). Purple shading denotes the trilayer Crl₃ flake. **b**, Inset: the extracted critical field for spin-flip transition (black circles) and critical temperature (blue squares) as a function of pressure. The error bar is determined as in Fig. 2a. **c**, Tunnelling current versus magnetic field at 2.45 GPa. Inset: tunnelling current measured while sweeping bias up (red) and down (blue). The sudden rise implies an irreversible change in sample configuration. Two magnetic phases, AFM I and AFM II, coexist at low fields (see text for details). **d**, Tunnelling current versus magnetic field measured after this switching event. Insets show only one of two possible AFM II magnetic configurations for the low-current level, as mentioned in the text. Also shown in the inset is a close-up view of the region indicated. Background quantum oscillations originate from the multilayer graphene contacts.

label $\uparrow\downarrow\uparrow$ and $\downarrow\uparrow\downarrow$ with obvious notation. Figure 3a shows I_{ι} versus H at zero pressure for a trilayer MTJ device (device 3). Either ground state presents two anti-aligned spin filters in series which,

as in the bilayer case, produce a low-current plateau at low field. A spin-flip transition occurs at $\sim 1.6\,\mathrm{T}$ to a fully polarized state ($\uparrow\uparrow\uparrow$ or $\downarrow\downarrow\downarrow$), causing a sudden rise to a high-current plateau at higher

NATURE MATERIALS LETTERS

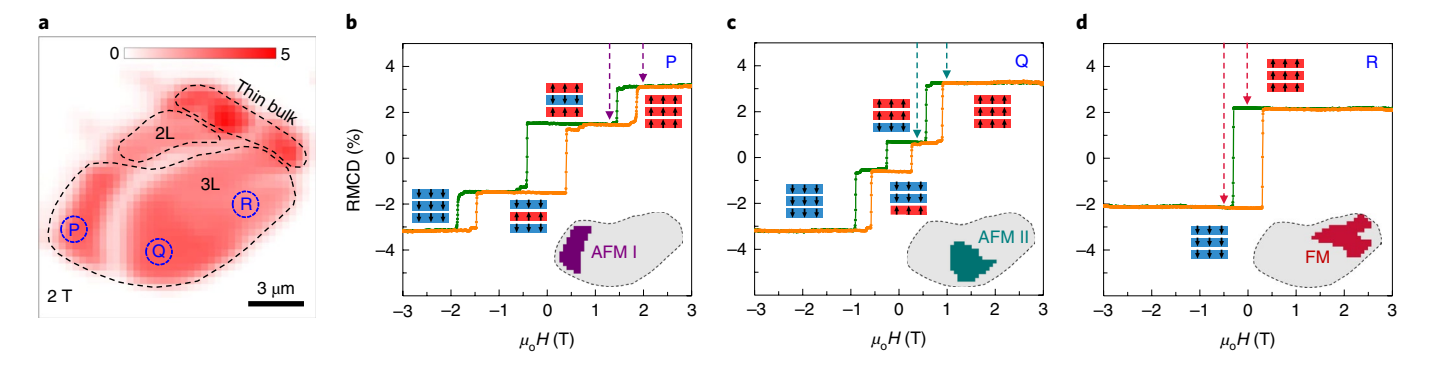


Fig. 4 | Magnetic and layer stacking phase map of a trilayer Crl₃ flake. a, Spatial map of RMCD signal at 2 T after sample removal from the pressure cell. Regions of varying thickness are labelled. The low-signal curved band corresponds to a crack in the sample. **b-d**, RMCD signal versus magnetic field at sites P, Q and R indicated in **a**, respectively. Insets: inferred magnetic states and the spatial maps identifying domains of each phase, in each case using the difference in RMCD signal between the two fields on the above trace. See Supplementary Fig. 6 for details. AFM I, both interfaces antiferromagnetically coupled; AFM II, one interface antiferromagnetically coupled and the other ferromagnetically coupled; FM, both interfaces ferromagnetically coupled. For phase AFM II there are two pairs of possible magnetic configurations, {↑↑↓, ↓↓↑} and {↓↑↑, ↑↓↓}, only the first of which is illustrated in **c**.

field. At a moderate applied pressure of 1.2 GPa (Fig. 3b), I_t –H traces have the same form as those at zero pressure but the critical field for spin-flip transition is increased. At the highest pressure of 2.45 GPa (Fig. 3c), this critical field peaks at 3.7 T, more than double the value at zero pressure (see inset in Fig. 3b, and Supplementary Fig. 4).

At high pressure, however, additional features appear that have not previously been seen in trilayer CrI₃. Figure 3c shows initial L-H traces at 2.45 GPa. In addition to the usual low- and high-field current levels we observe a new intermediate level, suggesting that another degree of freedom is involved. After performing these measurements, we swept the direct current bias while monitoring I, at a fixed magnetic field of $+1.3\,\mathrm{T}$, as shown in the inset in Fig. 3c. While first increasing the bias (red trace), at about $V = -300 \,\mathrm{mV}$, we observed a sudden increase in I, to a higher level. Thereafter, the current appeared to remain at the higher level as the bias was returned to zero (blue trace), indicating that a permanent change had occurred in the magnetic configuration. Such a permanent change could have been caused by a change in crystal structure, such as a reconfiguration of the stacking. Figure 3d shows an I_t-H trace after this reconfiguration had occurred. The lower field increase is in the same position as before (1.7 T, Fig. 3c), but the higher field jump has disappeared and the current at low field roughly doubled. These observations can be explained naturally as follows.

Before current-induced reconfiguration (Fig. 3c), in the low-field current plateau the sample contains coexisting domains of two different layered antiferromagnetic phases, which we call AFM I and II. AFMI is the phase found in the pristine trilayer, with two antiferromagnetic interfaces and hence one time-reversal pair of ground states, $\{\uparrow\downarrow\uparrow,\downarrow\uparrow\downarrow\}$. AFM II is a new phase, having one antiferromagnetic and one ferromagnetic interface, with two time-reversal pairs of possible magnetic configurations, $\{\uparrow\uparrow\downarrow,\downarrow\downarrow\uparrow\}$ and $\{\downarrow\uparrow\uparrow,\uparrow\downarrow\downarrow\}$. This situation could have occurred as a result of a change in the stacking at just one of the two interlayer interfaces, with consequences similar to those for the single interface in the bilayer. The case with the upper interface ferromagnetic and lower antiferromagnetic is sketched as one of the insets in Fig. 3c. In either AFMI or II, as the field is increased at some point the Zeeman energy overcomes the antiferromagnetic coupling to produce a spin-flip transition. Since AFM II has only one antiferromagnetic interface, the AFM II domains flip to the fully polarized configuration at a lower field of 1.7 T, resulting in the intermediate current level. Since AFMI has two antiferromagnetic interfaces, the AFMI domains switch at roughly double the field, 3.7 T, to leave the sample fully polarized and result in the highest current level. After the current-induced reconfiguration (Fig. 3d), the disappearance of only the 3.7-T rise

implies that most AFMI has been converted to AFMII. Closer inspection of Fig. 3d nevertheless reveals a tiny hysteresis remaining up to the higher critical field, indicating that a small amount of AFMI is still present.

After removing device 3 from the pressure cell, we performed spatially resolved RMCD measurements that confirmed the presence of multiple magnetic phases. Figure 4a shows a spatial map of the RMCD signal at a fixed field of 2T, which is sufficient for full polarization of CrI₃. (Note that, in addition to trilayer, we also see bi- and multilayer regions in this sample; see Supplementary Fig. 5.) Figure 4b-d shows the RMCD signal as a function of magnetic field at the three indicated laser site positions. At position P (Fig. 4b), RMCD exhibits the three-flip AFM I behaviour of a pristine exfoliated trilayer. At position Q (Fig. 4c), near the tunnel junction area, there are again three spin-flip transitions but they occur at fields about half those for the pristine trilayer. This suggests that the magnetic state at Q is AFM II, consistent with the assignment from the tunnelling measurements. At position R (Fig. 4d), the RMCD signal shows a single hysteresis loop centred at zero field, characteristic of a ferromagnetic phase in which both interfaces in the trilayer have ferromagnetic coupling.

The different spin-flip transition fields can be used to uniquely identify domains of different phases. For example, when the field is swept down from 2.0 to 1.3 T, only AFMI has a spin-flip transition, with a change in RMCD signal of about 1.3%. A map of AFMI domains can therefore be created by mapping the RMCD signal at these two fields and identifying the regions where the signal is different in the two cases (inset in Fig. 4b). A similar procedure yields maps of the AFMII and fully ferromagnetic domains (insets in Fig. 4c,d, respectively; details are given in Supplementary Fig. 6).

The existence of three different magnetic phases implies that at least three different stacking configurations in trilayer CrI₃ can be accessed by application of pressure. As in the bilayer case, results from polarization-resolved Raman spectroscopy are consistent with multiple stacking arrangement (Supplementary Fig. 5). The coexistence of the different stacking configurations is likely to involve inhomogeneity in the sample, which results in the conditions for the first-order transition varying from point to point. In future work, atomically resolved imaging (for example, transmission electron microscopy) could enable identification of exact stacking configurations, details of domain boundaries and their precise connections with the various magnetic states. Our work highlights CrI₃ as a model system for exploring reconfigurable magnetic structure via control of stacking, by either pressure or vdW assembly, potentially with the addition of twist-angle control. This suggests new

LETTERS NATURE MATERIALS

possibilities for engineering magnetism, such as the creation of designer real-space spin textures²⁹ and manipulation of magnetic order to control electronic phenomena—for example, in a layered Chern insulator such as MnBi₂Te₄.

Similar results have been reported in this issue of *Nature Materials*³⁰.

Online content

Any methods, additional references, Nature Research reporting summaries, source data, statements of code and data availability and associated accession codes are available at https://doi.org/10.1038/s41563-019-0505-2.

Received: 20 May 2019; Accepted: 11 September 2019; Published online: 28 October 2019

References

- Gong, C. et al. Discovery of intrinsic ferromagnetism in two-dimensional van der Waals crystals. Nature 546, 265–269 (2017).
- Huang, B. et al. Layer-dependent ferromagnetism in a van der Waals crystal down to the monolayer limit. Nature 546, 270–273 (2017).
- Burch, K. S., Mandrus, D. & Park, J.-G. Magnetism in two-dimensional van der Waals materials. Nature 563, 47–52 (2018).
- Jiang, P. et al. Stacking tunable interlayer magnetism in bilayer CrI₃. Phys. Rev. B 99, 144401 (2019).
- Soriano, D., Cardoso, C. & Fernández-Rossier, J. Interplay between interlayer exchange and stacking in CrI₃ bilayers. Solid State Commun. 299, 113662 (2019).
- Sivadas, N., Okamoto, S., Xu, X., Fennie, C. J. & Xiao, D. Stacking-dpendent magnetism in bilayer CrI₃. Nano Lett. 18, 7658–7664 (2018).
- Jang, S. W., Jeong, M. Y., Yoon, H., Ryee, S. & Han, M. J. Microscopic understanding of magnetic interactions in bilayer CrI₃. *Phys. Rev. Mater.* 3, 031001 (2019). (R).
- Wang, Z. et al. Very large tunneling magnetoresistance in layered magnetic semiconductor CrI₃. Nat. Commun. 9, 2516 (2018).
- Cao, H. B. et al. Low-temperature crystal and magnetic structure of RuCl₃. Phys. Rev. B 93, 134423 (2016).
- Subhan, F., Khan, I. & Hong, J. Pressure-induced ferromagnetism and enhanced perpendicular magnetic anisotropy of bilayer CrI₃. J. Phys. Condens. Matter 31, 355001 (2019).
- 11. Song, T. et al. Giant tunneling magnetoresistance in spin-filter van der Waals heterostructures. Science 360, 1214–1218 (2018).
- Klein, D. R. et al. Probing magnetism in 2D van der Waals crystalline insulators via electron tunneling. Science 360, 1218–1222 (2018).
- Kim, H. H. et al. One million percent tunnel magnetoresistance in a magnetic van der Waals heterostructure. Nano Lett. 18, 4885–4890 (2018).
- Klein, D. R. et al. Enhancement of interlayer exchange in an ultrathin two-dimensional magnet. *Nat. Phys.* https://doi.org/10.1038/s41567-019-0651-0 (2019).
- McGuire, M. A., Dixit, H., Cooper, V. R. & Sales, B. C. Coupling of crystal structure and magnetism in the layered, ferromagnetic insulator CrI₃. Chem. Mater. 27, 612–620 (2015).
- Sun, Z. et al. Giant nonreciprocal second-harmonic generation from antiferromagnetic bilayer CrI₃. Nature 572, 497–501 (2019).
- Thiel, L. et al. Probing magnetism in 2D materials at the nanoscale with single-spin microscopy. Science 364, 973–976 (2019).
- Yankowitz, M. et al. Dynamic band-structure tuning of graphene moiré superlattices with pressure. Nature 557, 404–408 (2018).
- Ci, P. et al. Quantifying van der Waals interactions in layered transition metal dichalcogenides from pressure-enhanced valence band splitting. *Nano Lett.* 17, 4982–4988 (2017).
- Zhao, Z. et al. Pressure induced metallization with absence of structural transition in layered molybdenum diselenide. Nat. Commun. 6, 7312 (2015).

- Yankowitz, M. et al. Tuning superconductivity in twisted bilayer graphene. Science 363, 1059–1064 (2019).
- Sun, Y. et al. Effects of hydrostatic pressure on spin-lattice coupling in two-dimensional ferromagnetic Cr₂Ge₂Te₆. Appl. Phys. Lett. 112, 072409 (2018).
- Son, S. et al. Bulk properties of the van der Waals hard ferromagnet VI₃. Phys. Rev. B 99, 041402 (2019).
- Lin, Z. et al. Pressure-induced spin reorientation transition in layered ferromagnetic insulator Cr₂Ge₂Te₆. Phys. Rev. Mater. 2, 051004 (2018).
- Mondal, S. et al. Effect of hydrostatic pressure on ferromagnetism in two-dimensional CrI₃. Phys. Rev. B 99, 180407 (2019).
- Gopinadhan, K. et al. Extremely large magnetoresistance in few-layer graphene/boron-nitride heterostructures. Nat. Commun. 6, 8337 (2015).
- Djurdjić-Mijin, S. et al. Lattice dynamics and phase transition in CrI₃ single crystals. Phys. Rev. B 98, 104307 (2018).
- Webster, L., Liang, L. & Yan, J.-A. Distinct spin–lattice and spin–phonon interactions in monolayer magnetic CrI₃. Phys. Chem. Chem. Phys. 20, 23546–23555 (2018).
- Tong, Q., Liu, F., Xiao, J. & Yao, W. Skyrmions in the moiré of van der Waals 2D magnets. Nano Lett. 18, 7194–7199 (2018).
- Li, T. et al. Pressure-controlled interlayer magnetism in atomically thin CrI₃. Nat. Mater. https://doi.org/10.1038/s41563-019-0506-1 (2019).

Acknowledgements

We thank S. Wu and W. Wu for the insightful discussion. This work was mainly supported by the Department of Energy, Basic Energy Sciences, Materials Sciences and Engineering Division, Pro-QM EFRC (grant no. DE-SC0019443). Device fabrication and quantum tunnelling measurement were partially supported by NSF MRSEC (grant no. 1719797), and magnetic circular dichroism measurement was partially supported by the Department of Energy, Basic Energy Sciences, Materials Sciences and Engineering Division (grant no. E-SC0018171). The material synthesis performed at the University of Washington was partially supported by the Gordon and Betty Moore Foundation's EPiQS Initiative (grant no. GBMF6759 to J.-H.C.). M.A.M. was supported by the US Department of Energy, Office of Science, Basic Energy Sciences, Materials Sciences and Engineering Division. K.W. and T.T. acknowledge support from the Elemental Strategy Initiative conducted by MEXT, Japan, A3 Foresight by JSPS and CREST (grant no. JPMJCR15F3) and JST. A portion of this work was performed at the National High Magnetic Field Laboratory, which is supported by National Science Foundation Cooperative Agreement (no. DMR-1644779) and the State of Florida. X.X. and J.-H.C. acknowledge support from the State of Washington-funded Clean Energy Institute. X.X. also acknowledges support from the Boeing Distinguished Professorship in Physics.

Author contributions

X.X., T.S., M.Y., C.R.D. and D.X. conceived the experiment. T.S. and Z.F. fabricated and characterized the devices, assisted by M.Y. and B.S. T.S., Z.F. and M.Y. performed the high-pressure measurements, assisted by D.G. T.S. performed magnetic circular dichroism and Raman measurements. K.H. and Q.Z. assisted in Raman measurement. T.S., Z.F., X.X., D.X., T.C. and D.H.C. analysed and interpreted the results. M.M., Z.L., Q.J. and J.-H.C. independently synthesized and characterized the bulk CrI₃ crystals. T.S., X.X., D.H.C., D.X. and Z.F. wrote the paper with input from all authors. All authors discussed the results.

Competing interests

The authors declare no competing interests.

Additional information

Supplementary information is available for this paper at https://doi.org/10.1038/s41563-019-0505-2.

Correspondence and requests for materials should be addressed to X.X.

Reprints and permissions information is available at www.nature.com/reprints.

Publisher's note Springer Nature remains neutral with regard to jurisdictional claims in published maps and institutional affiliations.

© The Author(s), under exclusive licence to Springer Nature Limited 2019

NATURE MATERIALS LETTERS

Methods

Device fabrication. Multilayer graphene and hBN flakes of 20-40 nm were mechanically exfoliated onto either 285- or 90-nm SiO₂/Si substrates and examined by optical and atomic force microscopy under ambient conditions. Only atomically clean and smooth flakes were used for device construction. V/Au (5/50 nm) metal electrodes were deposited on the bottom hBN flakes and substrates using a standard electron beam lithography with a bilayer resist (A4 495 and A4 950 poly (methyl methacrylate)) and electron beam evaporation. CrI₃ crystals were exfoliated onto 90-nm SiO₂/Si substrates in an inert gas glove box with water and oxygen concentration <0.5 ppm. CrI₃ flakes were identified by their optical contrast relative to the substrate using established optical contrast models of CrI₃ (ref. 2). The layer assembly was performed in the glove box using a polymer-based dry transfer technique. The flakes were picked up sequentially: top hBN, top graphene contact, CrI₃, bottom graphene contact. The resulting stacks were then transferred and released on top of the bottom hBN with pre-patterned electrodes. In the resulting heterostructure, the CrI₃ flake is fully encapsulated and the top/ bottom graphene flakes are connected to the prepatterned electrodes. Finally, the polymer was dissolved in chloroform for <1 min to minimize exposure to ambient conditions. The SiO₂/Si substrates were diced to approximately 1.7×1.7 mm² to fit within the inner bore of the pressure cell¹⁸.

Electrical measurements with pressure control. Electrical measurements at zero applied pressure were performed in a PPMS DynaCool cryostat (Quantum Design, Inc.) with a base temperature of 2 K. Measurements at high pressure were performed with a piston pressure cell in a VTI insert cryostat under similar experimental conditions. Figure 1c shows the schematic of the experimental set-up. For direct current measurement, a bias voltage (V) was applied to the top graphene contact with the bottom one grounded. The resulting tunnelling current (I) was amplified and measured by a current pre-amplifier (DL Instruments, 1211). For alternating current measurement, a standard lock-in technique was used by

applying $500-\mu V$ alternating current excitation at a relatively low frequency of about 13 Hz (with Stanford Research Systems SR830).

Hydrostatic pressure was applied using a pressure cell. The device was first glued to a metal stage using epoxy, then Pt wires were affixed to the gold contacts using silver paste. A Teflon cup was filled with the pressure medium (oil) and carefully fitted over the device and onto the stage, such that the device was completely encapsulated in oil. The stage/Teflon cup was then fitted into the inner bore of a piston cylinder cell and a hydraulic press was used to compress the top of the Teflon cup, which was held in place by a locking nut. The pressure cell was then loaded into a cryostat for electrical measurement. The in situ pressure was determined by measuring the fluorescence response of a ruby crystal in the cell through a thin optical fibre at both ambient and low temperature. Increasing or decreasing pressure requires warming the sample to room temperature and reloading the cell in the hydraulic press before cooling again. This technique closely follows a previous study on vdW heterostructures with pressure¹⁵.

Reflective magnetic circular dichroism and Raman spectroscopy

measurements. Reflective magnetic circular dichroism measurements were performed in a closed-cycle cryostat (attoDRY 2100) at a temperature of 2 K and an out-of-plane magnetic field up to 9 T. A 632.8-nm helium-neon laser was used to probe the device at normal incidence, with a fixed power of 100 nW. The alternating current lock-in measurement technique used to measure the RMCD signal closely followed the previous magneto-optical Kerr effect and RMCD measurements of the magnetic order in atomically thin CrI₃ (refs. ^{2,11}). Low-frequency Raman spectroscopy was performed with a 632.8-nm helium-neon laser at a temperature of either 80 or 270 K.

Data availability

The data that support the findings of this study are available from the corresponding author upon reasonable request.